Development 139, 3157-3167 (2012) doi:10.1242/dev.081174

Anterior-posterior differences in HoxD chromatin topology in limb development

Iain Williamson, Ragnhild Eskeland*, Laura A. Lettice, Alison E. Hill, Shelagh Boyle, Graeme R. Grimes, Robert E. Hill‡ and Wendy A. Bickmore‡

SUMMARY

A late phase of HoxD activation is crucial for the patterning and growth of distal structures across the anterior-posterior (A-P) limb axis of mammals. Polycomb complexes and chromatin compaction have been shown to regulate Hox loci along the main body axis in embryonic development, but the extent to which they have a role in limb-specific HoxD expression, an evolutionary adaptation defined by the activity of distal enhancer elements that drive expression of 5′ Hoxd genes, has yet to be fully elucidated. We reveal two levels of chromatin topology that differentiate distal limb A-P HoxD activity. Using both immortalised cell lines derived from posterior and anterior regions of distal E10.5 mouse limb buds, and analysis in E10.5 dissected limb buds themselves, we show that there is a loss of polycomb-catalysed H3K27me3 histone modification and a chromatin decompaction over HoxD in the distal posterior limb compared with anterior. Moreover, we show that the global control region (GCR) long-range enhancer spatially colocalises with the 5′ HoxD genomic region specifically in the distal posterior limb. This is consistent with the formation of a chromatin loop between 5′ HoxD and the GCR regulatory module at the time and place of distal limb bud development when the GCR participates in initiating Hoxd gene quantitative collinearity and *Hoxd13* expression. This is the first example of A-P differences in chromatin compaction and chromatin looping in the development of the mammalian secondary body axis (limb).

KEY WORDS: Autopod, Enhancer, Polycomb, Mouse

INTRODUCTION

Regulated Hox gene expression is important in anterior-posterior (A-P) patterning of the primary embryonic axis, with Hox genes being first activated at gastrulation (Wyngaarden et al., 2011; Deschamps and van Nes, 2005). The HoxD cluster has also been co-opted more recently in evolution into regulating the growth and patterning of the limb and digits.

Polycomb repressive complexes (PRC1 and PRC2) are required to maintain Hox genes in a silent compact chromatin state in embryonic stem (ES) cells (Boyer et al., 2006; Lee et al., 2006; Endoh et al., 2008; Stock et al., 2007; Eskeland et al., 2010). Whereas roles of polycomb at Hox loci are well established in early embryonic development and in differentiation along the primary embryonic axis (Voncken et al., 2003; Faust et al., 1998; Chambeyron et al., 2005; Soshnikova and Duboule, 2009), whether polycomb-mediated chromatin changes are involved in Hox regulation in the secondary body axis is unclear.

Two phases of Hoxd expression are important in limb development and patterning (Tarchini and Duboule, 2006; Zakany and Duboule, 2007). The first phase results in expression of 3′ Hoxd genes (*Hoxd1-9*) earlier than the 5′ genes. This restricts 5′ HoxD expression to the posterior side of the distal limb bud and is required for limb outgrowth, proximal limb development, limb A-P polarity and the posterior expression of sonic hedgehog (*Shh*). This 3′-5′ temporal and spatial collinearity is reminiscent of regulation in the main embryonic axis, which is accompanied by progressive loss of histone H3 lysine 27 tri-methylation (H3K27me3) catalysed by PRC2 (Soshnikova and Duboule, 2009). However, it might also require as yet undefined regulatory elements 3′ of HoxD (Spitz et al., 2005).

A later phase [embryonic day (E) 10.5] of Hoxd expression in the distal limb is required for digit morphogenesis (Spitz et al., 2003). This is characterised by ‘quantitative collinearity’ in which expression of the most 5′ gene, *Hoxd13*, is initially strongest in the posterior distal mesenchyme, with progressively less strong expression of *Hoxd12* to *Hoxd10*. The *Hoxd13* expression domain then spreads anteriorly, so that by E12.5 it is the only Hoxd gene for which expression is robust enough to be detectable on the most anterior side (Montavon et al., 2008). This is driven by enhancer elements including a ~40 kb global control region (GCR) located 180 kb 5′ (centromeric) of *Hoxd13* beyond *Evx2* and *Lnp*, and the Prox enhancer located between *Evx2* and *Lnp* (Fig. 4A) (Spitz et al., 2003; Tschopp and Duboule, 2011). It is not clear whether late phase HoxD regulation involves polycomb-mediated repression.

Here, we use immortalised mesenchymal cells derived from either the anterior (A) or the posterior (P) distal limb of E10.5 embryos, which show high levels of *Hoxd13* expression in the posterior-derived cells, to show that the ancestral role of polycomb in regulating the HoxD cluster appears to be maintained during distal limb development. There is a loss of H3K27me3 and a decompaction of higher order chromatin structure over HoxD in the distal posterior, compared with the anterior, limb cells. This is confirmed by analysis in dissected limb buds. Furthermore, we show a spatial colocalisation of the GCR and 5′ HoxD that is restricted to the distal posterior limb, consistent with the notion of physical association between this enhancer and its target genes. This is the first demonstration of differential chromatin compaction and enhancer-gene colocalisation across the A-P axis of the developing limb.

MRC Human Genetics Unit, MRC Institute of Genetics and Molecular Medicine, University of Edinburgh, Crewe Road, Edinburgh EH4 2XU, UK.

*Present address: Department of Molecular Biosciences, University of Oslo, N-0316 Oslo, Norway
‡Authors for correspondence (Bob.Hill@igmm.ed.ac.uk; Wendy.Bickmore@igmm.ed.ac.uk)

Accepted 8 June 2012

MATERIALS AND METHODS

Immortomouse cell lines

The posterior third and the anterior two thirds of distal forelimb buds were dissected from E10.5 mouse embryos from an Immortomouse (H-2kb-tsA58) × CD1 cross (Jat et al., 1991). After washing in PBS, limb buds were treated using trypsin (0.2 g/l)/Versene for 15-20 minutes, and dispersed gently. Cells were plated into 6-well plates in DMEM, 10% foetal calf serum, 20 ng/ml γ-Interferon (Peprotech) and grown at 33°C, the permissive temperature for the temperature-sensitive T antigen. A1/P1 and A2/P2 cell lines pairs were derived from separate litters.

RNA expression

RNA was prepared using Trizol reagent (Invitrogen) according to the manufacturer's protocol [for limb buds, dissected anterior and posterior tissue was dissociated into single cells in Trizol using a syringe with a 25G (0.5 mm) needle (BD Microlance)], followed by phenol:chloroform extraction and digestion with 2U DNaseI (Ambion) for 30 minutes at 37°C. cDNA was made using a First Strand Synthesis Kit (Roche) and amplified by PCR or real-time qRT-PCR using specific primers (supplementary material Table S1).

For expression arrays, 400 ng of RNA from A2/P2 cells were amplified using the Illumina TotalPrep RNA Amplification Kit (Ambion). Amplified, biotinylated cRNAs (1.5 μg) were labelled and hybridised to Illumina MouseRef6 Gene Expression beadchip arrays [Gene Expression Omnibus (GEO) accession platform number GPL6887, expression data GSE38370]. Data were analysed in R using limma (Smyth et al., 2005) and beadarray (Dunning et al., 2007) bioconductor packages. Probes with detection *P*-values less than 0.01 were removed from further analysis. Signals were quantile normalised to remove technical variation, and differential expression was assessed using limma's lmFit, eBayes and topTable function. *P*-values were corrected for multiple testing (Benjamini and Hochberg, 1995).

The 5944 genes with significantly differential A:P expression (adjusted $P<0.05$) were ranked by *P*-value and searched for enriched gene ontology (GO) terms using the Gene Ontology enrichment analysis and visualisation tool (GOrilla) (Eden et al., 2009). To avoid false positives $P<10^{-7}$ was set as the cut off for terms to be considered, based on the Bonferroni correction.

Acid extraction of histones and western blot analysis

Nuclei were isolated from 3-6×10^6 cells and histones acid-extracted and analysed as described (Eskeland et al., 2010).

Chromatin immunoprecipitation

Native chromatin immunoprecipitation (nChIP) from cell lines was performed as previously described (Eskeland et al., 2010), except that 40-46 Boehringer units of MNase (Worthington) was used to digest 1-6×10^8 cells.

For tissue, distal anterior and posterior forelimb buds were dissected from 50-55 E10.5 embryos. Owing to the lower cell numbers (~1×10^6), nChIP was performed with the following modifications: cells were digested with 8-9 Boehringer units of MNase (Worthington). Released chromatin (10-30 μg) was incubated with 3-5 μg prebound (to Protein A or G magnetic beads, Invitrogen) H3K27me3 antibody (Millipore) in the presence of 25 μg BSA for 3 hours at 4°C.

For Ring1B ChIP, 0.5-3×10^7 anterior and posterior limb tissue cells dissected from the distal forelimb buds of 70-75 E10.5 embryos were fixed with 1% formaldehyde (25°C, 10 minutes) and stopped with 0.125 M glycine. Sonication was as described (Eskeland et al., 2010). Released chromatin (30-50 μg) was incubated with 1 μg of prebound (Protein A magnetic beads, Invitrogen) Ring1B antibody (MBL, D139-3) or mouse IgG (Santa Cruz, sc-2025).

ChIP analysis

Relative quantification of ChIP by qPCR was as previously described (Eskeland et al., 2010) using primers described in supplementary material Table S2.

Input or ChIP DNA (10 ng) was amplified using the WGA2 Whole Genome Amplification Kit (Sigma) and labelled with Cy3 or Cy5 by random priming according to the NimbleGen ChIP-chip protocol (Roche). Two or three biological replicates, with dye swaps, were hybridised for 20 hours to a custom 3×720 K mouse tiling array (NimbleGen, Roche) containing 179,493 unique probes from different genomic regions, with each probe represented by four replicates (GEO accession platform number GPL14936, array data GSE38526). Arrays were washed according to the manufacturer's protocol and scanned on a NimbleGen MS 200 Microarray scanner (Roche) using 100% laser power and 2 μm resolution. Raw signal intensities were quantified from TIFF images using MS 200 Data Collection software.

Microarray data were analysed and ChIP enrichments determined as described by Pradeepa et al. (Pradeepa et al., 2012). To determine the significance of the difference in H3K27me3 enrichment over HoxD in anterior versus posterior limb tissue cells, the median log enrichment value of probes covering the locus or specific locus sub-regions (5′, 3′; promoters, genes, intergenic regions) were calculated. The statistical significance of any A:P differences were assessed using the non-parametric Mann-Whitney U-test. Mean log enrichment values were used to compare individual genes and promoter regions within HoxD, and adjacent genes and statistical significance was assessed using the two-sample Student's *t*-test.

Fluorescence in situ hybridisation (FISH)

2D FISH was as described previously (Chambeyron and Bickmore, 2004; Eskeland et al., 2010). Fosmid clones (supplementary material Table S3) were prepared and labelled as previously described (Morey et al., 2007). Between 80 and 120 ng of biotin- and digoxigenin-labelled probe were used per slide, with 8-12 μg of mouse Cot-1 DNA (Invitrogen) and 10 μg salmon sperm DNA.

For 3D FISH, E10.5-11 embryos from CD1 mice were collected, fixed, embedded, sectioned and processed as previously described (Morey et al., 2007), except that sections were cut at 6 μm.

Image analysis

For 2D FISH, slides were analysed as described (Morey et al., 2007) except that the Chroma #83000 triple band pass filter set (Chroma Technology Corporation, Rockingham, VT, USA) and a motorised filter wheel (Prior Scientific Instruments, Cambridge, UK) were used.

For 3D analysis of tissue sections, slides were imaged with a Hamamatsu Orca AG CCD camera (Hamamatsu Photonics, Welwyn Garden City, UK), Zeiss Axioplan II fluorescence microscope with Plan-neofluar or Plan apochromat objectives, a Lumen 200W metal halide light source (Prior Scientific Instruments) and Chroma #89014ET single excitation and emission filters (Chroma Technology Corporation) with the excitation and emission filters installed in Prior motorised filter wheels. A piezoelectrically driven objective mount (PIFOC model P-721, Physik Instrumente, Karlsruhe, Germany) was used to control movement in the *z* dimension. Hardware control, image capture and analysis were performed using Volocity (PerkinElmer, Waltham, MA, USA). Images were deconvolved using a calculated point spread function with the constrained iterative algorithm of Volocity. Image analysis was carried out using the Quantitation module.

RESULTS

Cell lines derived from the mesenchyme of E10.5 limb buds

Activity of limb enhancers in the HoxD GCR first becomes apparent in posterior mesenchyme cells of the distal forelimb bud at E10.5, followed later by anterior extension of this expression zone across the distal limb (Spitz et al., 2003). Therefore, we restricted our analysis to E10.5 limb buds to capture the initiation of this second wave of HoxD regulation.

Analysing chromatin structure in the small number of cells dissected from mouse embryos is challenging (Soshnikova and Duboule, 2009). However, conditionally immortalised cell lines

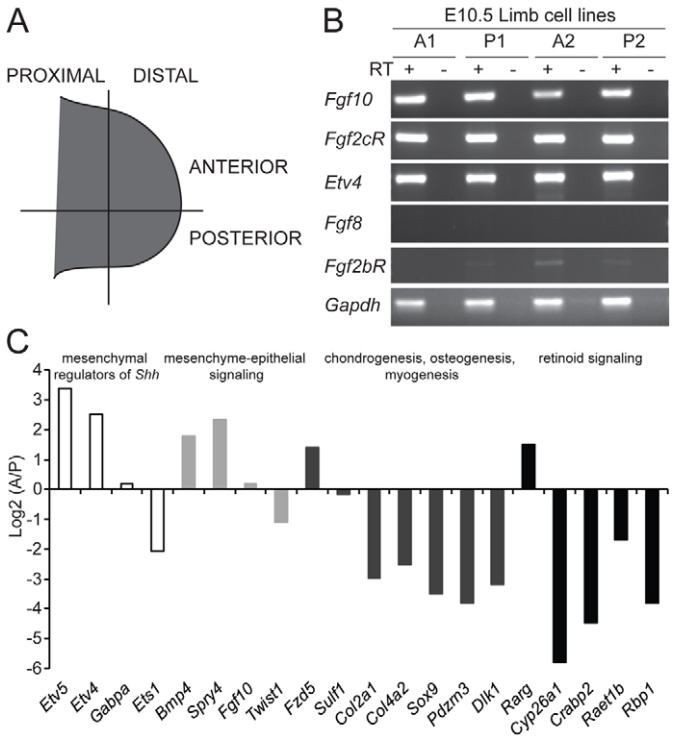

Fig. 1. Characterisation of cell lines from distal posterior and anterior mouse forelimb. (**A**) Schematic of E10.5 forelimb bud showing the dissection into anterior (A) and posterior (P) distal regions. (**B**) RT-PCR to detect the expression of mesenchymal (*Fgf10*, *Fgf2cR*, *Etv4*) and epithelial (*Fgf8*, *Fgf2cR*) markers in immortomouse cell lines derived from the anterior (A) or posterior (P). The two cell line pairs derive from embryos from different litters. Primer sequences are indicated in supplementary material Table S1. –, negative control lacking reverse transcriptase. (**C**) Log2 A/P expression from microarray analysis of A2/P2 cells for selected genes categorised according to their function.

can be derived from the transgenic 'immortomouse', which expresses temperature-sensitive SV40 T antigen (Jat et al., 1991). Such cell lines appear to retain many biological properties of the cells from which they were derived, including gene expression patterns and response to signalling pathways (Kohn et al., 2010). We derived two sets of cell lines from dissected E10.5 forelimb buds to represent the most posterior third of the distal limb (cell lines P1 and P2) or the anterior two-thirds (A1 and A2) (Fig. 1A).

The embryonic limb bud consists of two main cell types: mesenchyme and the surface ectoderm, which at the most distal margin forms the apical ectodermal ridge (AER). The morphology of the cell lines indicated that they were likely to be mesenchymal in origin and RT-PCR analysis confirmed this (Fig. 1B). *Fgf10* is expressed in limb bud mesenchyme and signals to the Fgfr2b receptor expressed in the AER to induce expression of *Fgf8* there. By contrast, *Fgfr2c* is expressed in both the mesoderm and ectoderm of the developing limb bud (Lizarraga et al., 1999; Duboc and Logan, 2011). The detection of mRNAs from *Fgf10* and *Fgfr2c*, but not *Fgf8* or *Fgfr2b* in immortomouse-derived limb bud cell lines thus indicates their derivation from the limb mesenchyme (Fig. 1B). The origin of these cells from the distal, rather than proximal, margin of the limb is supported by the expression of *Etv4* (Mao et al., 2009). Analysis by expression microarrays provided further evidence for this. Genes with proximally restricted expression domains, such as *Tbx15*, *Cart1* (*Alx1* – Mouse Genome Informatics), *Emx2*, *Pax1* (chondrogenesis), *Pax3* (myogenesis) (Kuijper et al., 2005), *Vcan*, *Ebf2* (neurogenesis) (Krawchuk and Kania, 2008) and *Shox* (chondrogenesis, myogenesis, neurogenesis) (Vickerman et al., 2011), could not be detected (data not shown). We conclude that the four cell lines retain at least some of the specific developmental functions expected of their limb origin (Robert and Lallemand, 2006; Hill, 2007).

Expression microarrays provided further insight into the differences between the anterior- and posterior-derived cell lines (A2 and P2) (GEO accession number GSE38370). For example, levels of *Etv4* and *Etv5* mRNAs (known to be expressed in the distal limb mesenchyme and important for the posterior restriction of Shh expression) (Mao et al., 2009) were higher in the anterior cells than in posterior cells, whereas expression of other ETS factors that define the spatial boundary of *Shh* were higher in the posterior cells (*Ets1*) or similar (*Gabpa*) throughout the distal limb bud (Lettice et al., 2012) (Fig. 1C). Genes involved in mesenchymal-epithelial signalling and distal limb patterning were upregulated in anterior (*Bmp4*, *Spry4*) and posterior (*Twist1*) cells or expressed evenly across the A-P axis (*Fgf10*). Among the genes with the highest ratio of expression in the posterior cells were those involved in retinoid signalling, and in chondrogenesis, osteogenesis or myogenesis (Fig. 1C).

Gene ontology analysis (GOrilla) indicated that the most significantly different A/P expression levels were for genes enriched for GO Biological Process terms ($P<10^{-9}$) such as A-P axis and pattern specification, anatomical structure morphogenesis and embryonic skeletal system morphogenesis – categories that reflect the cell lines' origins from mesenchymal tissue of the A-P axis of a developing appendage (supplementary material Fig. S1).

Cell lines reflect differential 5′ Hoxd gene expression in distal posterior limb bud

Spatial expression domains of Hoxd genes in E10.5 limb buds are well characterised (Spitz et al., 2003; Spitz et al., 2005; Tarchini and Duboule, 2006; Zakany and Duboule, 2007). We used RT-PCR and qRT-PCR on both sets of cell lines and on tissue dissected from E10.5 anterior and posterior forelimb buds to determine how relevant the limb cell lines are for analysis of HoxD spatial regulation.

Hoxd1 mRNA was not detected in any of the cell lines and only very faintly in anterior limb tissue (Fig. 2A). *Hoxd3* expression was detected at generally low levels (Fig. 2A) that are similar between the anterior and posterior limb tissue and the corresponding cell lines, except for even lower levels in P2 cells (Fig. 2B). There was no significant A/P difference in *Hoxd3* expression in either cell line pairs or limb tissue (Fig. 2C). Conversely, at the 5′ end of HoxD, *Hoxd13* expression levels were 17-fold higher in posterior limb and limb-derived cell lines than in anterior equivalents (Fig. 2C). A2/ P2 cell lines showed expression levels similar to those in anterior and posterior tissue, but levels in A1/P1 were both proportionally lower (Fig. 2B). We observed slightly higher *Hoxd12* expression in the posterior limb tissue than in the anterior, and higher *Hoxd11* in P1 compared with A1 cells, but their expression levels of were both too low for reliable quantification. *Hoxd10* expression showed a high A/P difference in both cell line pairs; the apparent large difference (Fig. 2C) measured in the A1/P1 cell lines is due to the very low expression levels in A1. *Hoxd8* expression showed an A/P differential (threefold higher in P2 than in A2) in the second cell line pair only due to its increased expression in P2 cells, expression

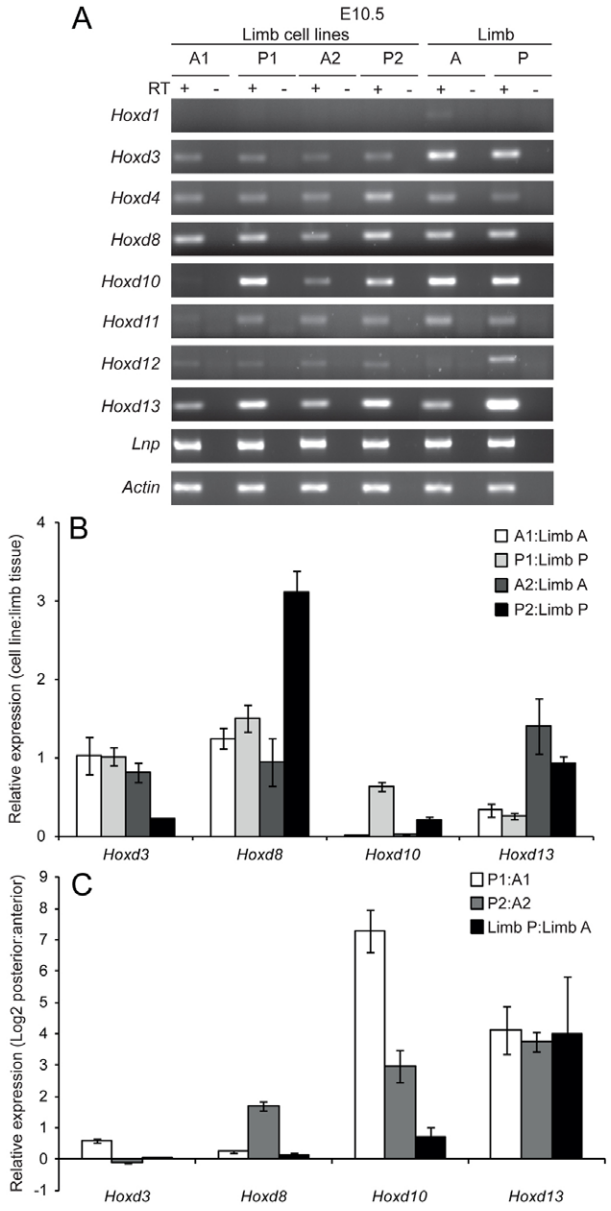

Fig. 2. Hoxd expression in distal anterior and posterior limb cell lines and mouse tissue. (**A**) RT-PCR to detect the expression of 3′ (*Hoxd1*, *Hoxd3*, *Hoxd4*, *Hoxd8*) and 5′ (*Hoxd10*, *Hoxd11*, *Hoxd12*, *Hoxd13*) Hoxd genes and the adjacent *Lnp* in both sets of cell lines (A1/P1, A2/P2) and in E10.5 distal forelimb tissue (A and P). Primer sequences are indicated in supplementary material Table S1. (**B**,**C**) Quantitative (q)RT-PCR to compare expression levels of 3′ (*Hoxd3*, *Hoxd8*) and 5′ (*Hoxd10*, *Hoxd13*) Hoxd genes in both sets of cell lines and in anterior or posterior distal forelimb tissue. (B) Expression in each cell line compared with the corresponding limb tissue. (C) Log2 P/A expression for both sets of cell lines (white and grey bars) and in distal forelimb tissue (black bars).

levels in A2, A1 and P1 being similar to limb tissue (Fig. 2B,C). No A/P difference in *Hoxd8* expression was detected in the E10.5 limb tissue. This suggests that both cell line pairs capture cells that have activated 5′ Hoxd genes specifically in the posterior compartment at the start of the second wave of HoxD activation in the distal limb and that this activation has a greater extension 3′ in the 2P cell line (to *Hoxd8*) than it does in 1P cells (*Hoxd10*). Gene activation extends more 3′ in both posterior-derived cell lines than in the limb tissue. This could be due to the outgrowth of cells that have more extensive gene activation than the average in the posterior limb or, more likely, that the regulatory mechanisms driving progressive 5′-3′ HoxD activation continue operating for some time after tissue dissection and during cell immortalisation.

Beyond *Hoxd13*, *Evx2* expression was not be detected in cell lines (data not shown) suggesting that the cells might originate from outside of the small *Evx2* expression domain at the extreme distal margin of the E10.5 forelimb bud (Tarchini and Duboule, 2006). *Shh* expression was also not detected, suggesting that it is not required for maintenance of the second wave of HoxD activation, at least in cell lines, as has been previously proposed (Harfe et al., 2004).

Although both immortomouse-derived distal limb cell line pairs show an A/P difference in 5′ HoxD activity, the A2/P2 pair show a more extensive domain of activation (*Hoxd13* to *Hoxd8*) and so were chosen for further study.

Loss of H3K27me3 over the HoxD cluster in posterior cells

The PRC2 polycomb complex is fundamental to regulation of Hox gene clusters during ES cell differentiation and early embryogenesis and is responsible for blanketing HoxD with H3K27me3 (Boyer et al., 2006; Lee et al., 2006). Polarised (3′-5′) loss of H3K27me3 accompanies 3′ Hoxd gene activation during ES cell differentiation (Eskeland et al., 2010) and in the tail bud of the primary axis during early embryogenesis (Soshnikova and Duboule, 2009). PRC2 function in the limb is required for cell survival and for proximodistal elongation of the limb (Wyngaarden et al., 2011), but whether differential polycomb-mediated chromatin changes are involved in regulating A-P Hoxd gene expression during the late phase of distal limb patterning is unclear.

Immunoblotting shows similar H3K27me3 levels globally in A2 and P2 cells (Fig. 3A). Using native ChIP (nChIP) combined with custom high-density tiling arrays covering multiple regions of the mouse genome, including Hox loci (Eskeland et al., 2010), we determined the H3K27me3 profile of the A2/P2 distal forelimb-derived cell lines (Fig. 3B) (GEO accession number GSE38526).

H3K27me3 is pervasive over HoxD in anterior cells, with both the 5′ and 3′ (*Hoxd1-d4*) genes densely covered (Fig. 3B). The dip in H3K27me3 between *Hoxd4* and *Hoxd8*, is similar to that seen in ES cells (Eskeland et al., 2010). Whereas H3K27me3 still blankets *Hoxd1-d3* in posterior (P2) cells, it is largely absent over the 5′ genes (Fig. 3B,C, upper two tracks). Beyond *Hoxd13*, H3K27me3 covers *Evx2* in both cell lines. In contrast to ES cells, in which both HoxB and HoxD loci are both blanketed (Eskeland et al., 2010), H3K27me3 is largely absent from HoxB in A2 and P2 cell lines, with only *Hoxb13* enriched, emphasising the particular regulation of HoxD across the A-P limb axis. As controls, the *Pax6* polycomb target was blanketed with H3K27me3 in both anterior and posterior, whereas H3K27me3 was absent from the widely expressed *Brd3*.

Of those arrayed probes significantly enriched in H3K27me3 in anterior cells (log2 H3K27me3/input≥1) (Fig. 3E, upper pie chart) only 8% are from HoxD. Yet 93% of probes with an at least twofold (log2≥1) A/P difference in H3K27me3 enrichment are from this locus and 88% are from 5′ HoxD (Fig. 3E, lower pie chart). By contrast, only 2% of probes with at least twofold A/P H3K27me3 difference are from HoxA. Therefore, extensive A/P differences in H3K27me3 are specific to HoxD in these cell lines. Quantitative PCR (qPCR) confirmed the lower H3K27me3 levels in P2 versus A2

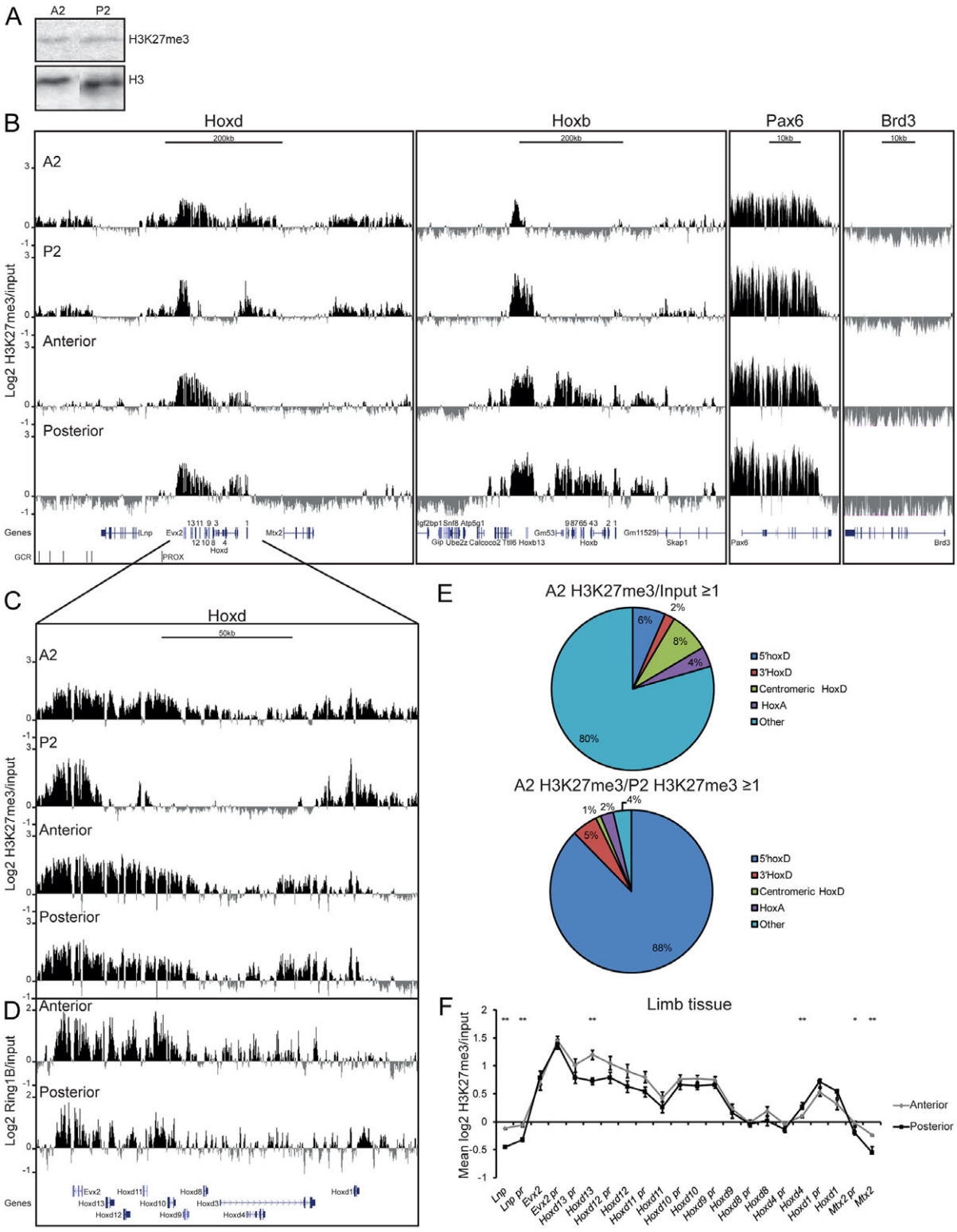

Fig. 3. H3K27me3 and Ring1B distribution in E10.5 limb cell lines and mouse forelimb tissue. (**A**) Western blot of H3K27me3 in A2 and P2 cells. Levels of H3 are shown for comparison. (**B**) Mean log2 H3K27me3/input at HoxD, HoxB, *Pax6* and *Brd3* loci in A2 and P2 cell lines (top two rows, *n*=2 biological replicates) and for anterior and posterior forelimb tissue (bottom two rows, *n*=4 – 2 biological and 2 technical – replicates). (**C**) As in B, but with an expanded view of the HoxD cluster. (**D**) Mean log2 Ring1B/input at the HoxD region for anterior and posterior forelimb tissue. *n*=2 biological replicates. (**E**) Pie charts showing the genomic distribution of different probes categories enriched for: (top) H3K27me3 in A2 cells (log2 H3K27me3/input≥1) versus (bottom) the proportion with an A2/P2 difference of log2≥1. (**F**) Mean (± s.e.m.) log2 H3K27me3/input at HoxD and neighbouring genes and promoters in distal forelimb anterior and posterior tissue. Average log2 values were calculated from each individual probe value that covered the genomic locations. The statistical significance of A:P differences in H3K27me3 enrichment over each gene and promoter were examined by two-sample *t*-test (**P*<0.01, ***P*<0.0001).

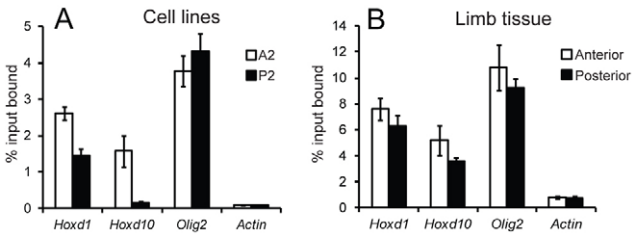

Fig. 4. Confirmation of A/P differences in H3K27me3 enrichment. (**A**) qPCR analysis of ChIP for H3K27me3 at *Hoxd1*, *Hoxd10*, *Olig2* and *Actb* (Actin) promoters in A2 (white) and P2 (black) cells. Enrichment is shown as mean percent input bound ± s.e.m. over three biological replicates. (**B**) As in A, but from E10.5 distal anterior (white) and posterior (black) forelimb tissue. *n*=2 biological replicates.

cells at *Hoxd10* (Fig. 4A), with a less dramatic decrease at *Hoxd1*. There was no significant A-P difference in H3K27me3 at *Olig2* (positive control) or *Actb* (β-actin, negative control).

The limb cell lines are apparently a relatively homogenous mesenchymal cell population. By contrast, more heterogeneous cell populations are inevitably present in dissected limb tissue, where AER- and differentiating mesenchyme-derived cells expressing different cohorts of Hoxd genes might mask differences in H3K27me3 levels between the anterior and posterior mesenchyme. Nevertheless, we analysed H3K27me3 in E10.5 anterior and posterior dissected distal forelimbs (Fig. 3B,C, lower two tracks) by nChIP. An H3K27me3 block covered the 3′ end of HoxD (*d1-d4*) in both limb regions. Both anterior and posterior limb samples also show a second block of modification over the 5′ end of HoxD, from *Hoxd9* through to *Evx2*, but this was at a significantly higher level in anterior compared with the posterior region (*Hoxd13-Hoxd10*; $P<0.0001$) (Fig. 3F; supplementary material Fig. S2A). Whereas in the anterior distal limb H3K27me3 remains high from *Evx2* to beyond *Hoxd12*, in the posterior H3K27me3 declines from the *Evx2-Hoxd13* intergenic region up to *Hoxd11* (Fig. 3C,F). This A-P difference in H3K27me3 levels in limb tissue is specific to 5′ HoxD (supplementary material Fig. S2B), being significantly greater ($P<0.0001$) than that for all Hox loci combined. The A-P difference for the 3′ HoxD region is not significant ($P=0.57$). H3K27me3 was more pervasive over the HoxB locus in cells dissected from the anterior or posterior limb tissues than in the cell lines (Fig. 3B), probably reflecting the heterogeneity of the former cell populations, and, unlike for HoxD, there were no differences between H3K27me3 at HoxB in anterior versus posterior limb.

Lower H3K27me3 levels at the *Hoxd10* promoter in the posterior versus anterior limb tissue cell populations was confirmed by qPCR, whereas levels at the *Hoxd1* promoter were similar in both distal limb samples (Fig. 4B). These data are consistent with a role for polycomb-mediated repression in regulating A-P differences in Hoxd expression during the patterning of the distal limb.

PRC1 levels are reduced over HoxD in distal posterior cells

The PRC1 complex recognises and binds to H3K27me3-modified chromatin to bring about chromatin compaction and gene repression. The ChIP profile of the PRC1 component Ring1B (Rnf2 – Mouse Genome Informatics) correlates with that of H3K27me3 in E10.5 anterior and posterior dissected limb bud tissues at HoxD (Fig. 3C,D), HoxB and *Pax6* (supplementary material Fig. S2C). A block of Ring1B extends from *Evx2* to *Hoxd9* in distal anterior limb, whereas in posterior tissue Ring1B coverage is more sparse over *Hoxd13-11*. The A/P difference in Ring1B levels was significant throughout 5′ HoxD (promoters, genes and intergenic; $P<0.0001$) (supplementary material Fig. S2D) and was greater than at all the Hox loci combined ($P<0.0001$) (supplementary material Fig. S2E).

A-P differences in chromatin compaction at HoxD in the distal limb bud

PRC1 brings about a chromatin compaction at target loci that is detectable by measuring the spatial separation of fluorescence in situ hybridisation (FISH) signals from closely apposed probe pairs (Eskeland et al., 2010) (Fig. 5A). Using these approaches, a decompaction of HoxD is seen as Hox genes are activated during ES cell differentiation and in the tail-bud of the embryo (Morey et al., 2007). We first used 2D FISH to assay chromatin compaction (d^2) across HoxD in limb bud cell lines. Any difference in inter-probe distances due to variation in nuclear size between cell lines was also assessed by normalising d^2 to the nuclear radius (r^2). However, in practice the same conclusions were reached when considering interprobe separation without normalisation to nuclear size (supplementary material Table S4).

Chromatin across HoxD (*Hoxd3-Hoxd13*) was significantly less compact in both distal posterior cell lines compared with the anterior cell lines ($P=0.0002$ and $P=0.03$ for A1/P1 and A2/P2, respectively) (Fig. 5B; supplementary material Table S4). This was restricted to the region with differential H3K27me3, as there is no significant A-P difference in compaction of the GCR-*Lnp* region 5′ of HoxD where similarly low levels of H3K27me3 are seen between A and P cell lines (Fig. 3B). Nor was there differential compaction at a control region around *Pax6* (*Rcn-Rpl10*) on the same chromosome (MMU2) as HoxD, and which contains genes with no known role in limb development and no differential expression between A and P cell lines.

We sought confirmation of differential HoxD compaction by 3D FISH in E10.5-11.0 embryo tissue sections cut through the anterior and posterior regions of the forelimb (Fig. 6A). Here, not only were we able to compare the distal anterior and posterior regions, but also more proximal limb regions and indeed the flank region adjacent to the forelimb bud tissue where Hoxd genes are not expressed. As observed in the cell lines, HoxD chromatin was significantly less compact (d^2) at the distal posterior forelimb bud compared with the distal anterior ($P=0.0008$) but also compared with other limb and non-limb regions analysed (proximal posterior, $P=0.02$; proximal anterior, $P=0.0002$; flank, $P=0.0002$) (Fig. 6B; supplementary material Table S5). There was no significant difference in HoxD chromatin compaction between any of the other limb regions or even between these other limb regions and the flank tissue. Likewise, no significant differences in chromatin compaction could be identified between any of the tissue regions, including the distal forelimb bud, at the GCR-*Lnp* and the *Rcn-Rpl10* control regions (Fig. 6B; supplementary material Table S5).

Analysis of the frequency of hybridisation signals separated by defined distance (d) intervals also demonstrates the less compact chromatin conformation of the HoxD locus compared with the adjacent GCR-*Lnp* region. The proportion of colocalised signals (<200 nm) was less for *Hoxd3-Hoxd13* than both GCR-*Lnp* (with a similar genomic distance) and the *Rcn-Rpl10* control region, which has a larger genomic distance separating the two probes (supplementary material Fig. S3). Conversely, the proportion of signal pairs >400 nm apart was greater for *Hoxd3-Hoxd13* than for the other two regions. The subpopulation of HoxD probe pairs separated by >600 nm

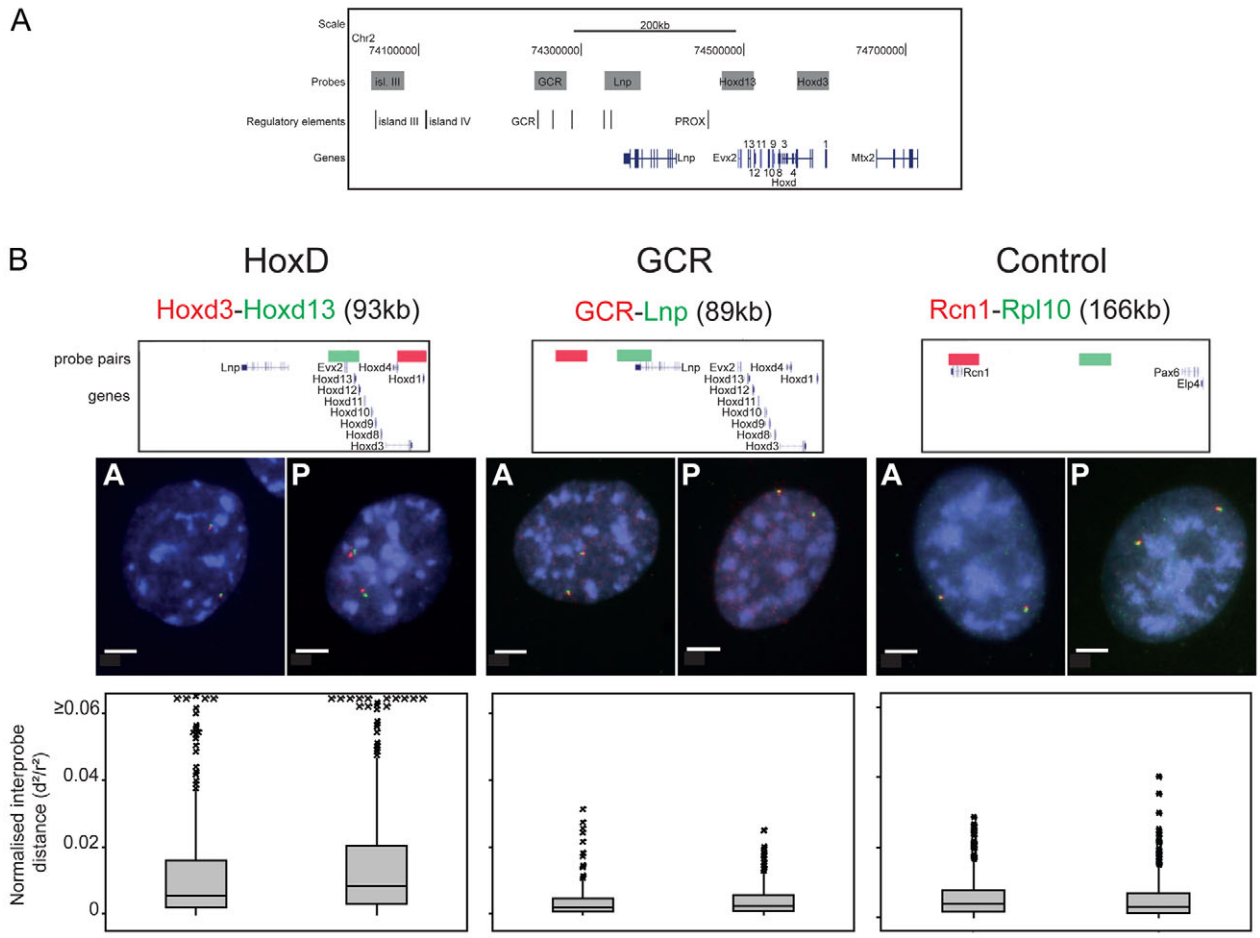

Fig. 5. Chromatin decompaction at HoxD in distal posterior limb cells. (**A**) Schematic of the genomic region around HoxD. The grey boxes above depict the probes used for FISH. Regulatory elements including the GCR and the PROX enhancer are also indicated. (**B**) 2D FISH with probe pairs at HoxD, the region centromeric to HoxD (GCR-*Lnp*) and a control region on MMU2, in A1 and P1 nuclei counterstained with DAPI (blue). Scale bars: 5 µm. Probe positions are shown above the images. Box plots show the distribution of interprobe distances (d^2) normalised to nuclear radius (r^2) for A1 and P1 cells. Shaded boxes show the median and interquartile range of data; crosses indicate outliers. *n*=~400 for HoxD, *n*=~300 for GCR, *n*=~300 for control. The statistical significance of differences were examined by Mann-Whitney U-tests (supplementary material Table S4).

(~25%) was significantly greater in the distal posterior forelimb compared with the rest of the limb regions and the adjacent flank (distal anterior, P=0.0001; proximal posterior, P=0.0001; proximal anterior, P=0.001; flank, P<0.0001) (supplementary material Fig. S3 and Table S6). We conclude that chromatin unfolding at HoxD accompanies the start of the second wave of Hoxd gene activation during limb development.

Nuclear colocalisation of the GCR and 5′ HoxD in distal posterior cells

Developmental stage E10.5 marks the start of the later phase of distal limb development, characterised by 'quantitative collinearity' in which strong expression of *Hoxd13* is initiated in the distal margin of the posterior mesenchyme. This is driven by enhancer elements located 5′ of HoxD, the best characterised of which is the GCR ~180 kb centromeric of *Hoxd13* (Fig. 3B, Fig. 5A) (Montavon et al., 2008).

One possible mechanism for long-range cis-regulation invokes the spatial colocalisation of the enhancer and target promoter (Williamson et al., 2011). Indeed, modelling of gene expression changes that occur as a consequence of 5′ HoxD deletions led to the suggestion that the first step in 5′ Hoxd gene activation in the distal posterior limb bud might be a long-range interaction (looping) between regulatory sequences such as GCR and the *Hoxd13* region (Montavon et al., 2008). To test this model, we analysed the hybridisation signals for the GCR and *Hoxd13* regions and determined the proportion that colocalised (d<200nm). Multiple areas within the E11.0 limb bud were analysed (Fig. 7A), including those where late phase gene activation initiates (distal posterior); where it is poised for later activation (distal anterior); where the early phase of 3′-5′ *Hoxd* gene activation, which does not depend on the GCR, has occurred (proximal limb); and then in the control flank mesoderm.

In contrast to the *Hoxd3-d13* region, average GCR-*Hoxd13* interprobe distances (d^2) were significantly smaller in the posterior distal limb bud compared with distal anterior (P=0.04) and also compared with the flank (P<0.0001), the proximal anterior (P=0.02) and proximal posterior (P=0.002) (Fig. 7B; supplementary material Table S7). This was not seen for distances between GCR and a probe at the 3′ end of *Lnp* (Fig. 6B) indicating that there is not a simple compaction of the whole region 5′ of *Hoxd13*. Moreover, the proportion of alleles for which GCR and *Hoxd13* probe signals were spatially colocalised (d<200nm) was far higher in posterior distal limb (>30%) than in all other areas

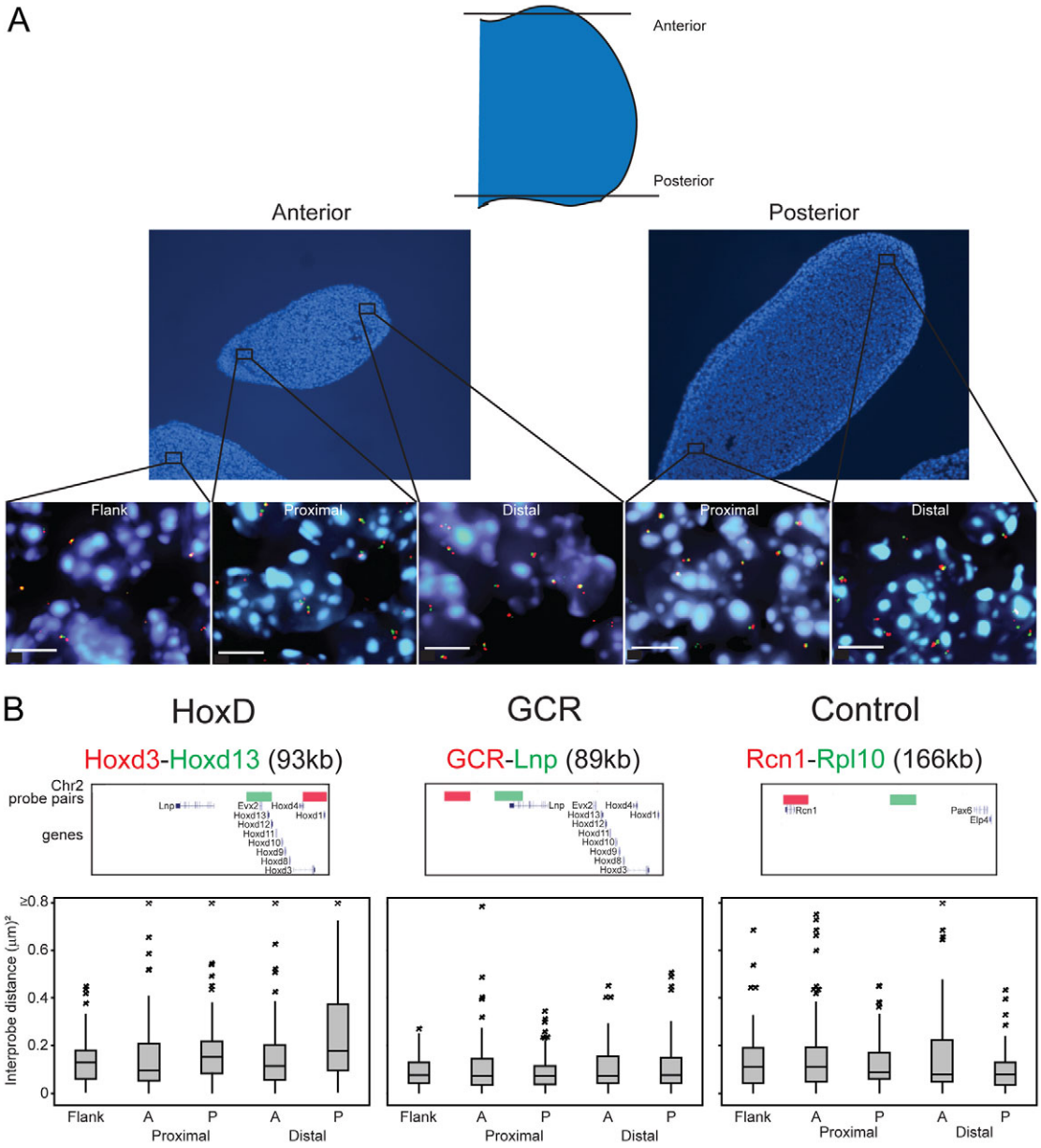

Fig. 6. Decompaction of HoxD specific to the distal posterior region of E11 mouse forelimbs. (**A**) FISH on anterior and posterior tissue sections. Schematic above indicates the position and plane of the sections. Below are examples of nuclei from each of the limb regions and the adjacent flank, hybridised with HoxD probe pairs. Scale bars: 5 μm. (**B**) Box plots show the distribution of interprobe distances (d^2) at the HoxD, GCR and control loci for the proximal and distal anterior and posterior forelimb bud and the adjacent flank. *n*=100 for HoxD, *n*>80 for GCR, *n*>80 for control. Probe positions as indicated in Fig. 5A. Statistical analysis is shown in supplementary material Table S5.

tested (Fig. 7C; supplementary material Fig. S4A and Table S8). These data are consistent with the formation of a chromatin loop between *Hoxd13* and the GCR regulatory module at the time and place of distal limb bud development when the GCR participates in initiating HoxD collinearity and *Hoxd13* expression.

Recently, 4C analysis was used to identify sequences that could be captured together with *Hoxd13* by cross-linking in tissue from across the distal limb at E12.5, a later stage of limb development than that studied here (Montavon et al., 2011). This identified multiple new potential regulatory regions in the extensive gene desert centromeric of HoxD and located far beyond the GCR. It was suggested that these elements might simultaneously interact with each other and with 5′ HoxD in the distal limb to form a compact regulatory hub. One of these new elements, island III, is ~200 kb centromeric of the GCR. We measured the physical separation between the island III region and the GCR – a genomic distance equivalent to that separating GCR from *Hoxd13* (~200 kb) – and also between the island III region and *Hoxd13* (Fig. 5A) in E11.0 limb buds. We did not detect any significantly increased frequency of colocalisation between island III and *Hoxd13* or between island III and GCR in posterior distal limb, compared with other forelimb regions (Fig. 7C; supplementary material Fig. S4B,C and Table S8). However, average interprobe distances (d^2) between 5′ HoxD and island III are similar to those between 5′ HoxD-GCR and GCR-island III despite the former being double the genomic distance, and the compaction of the island III-Hoxd13

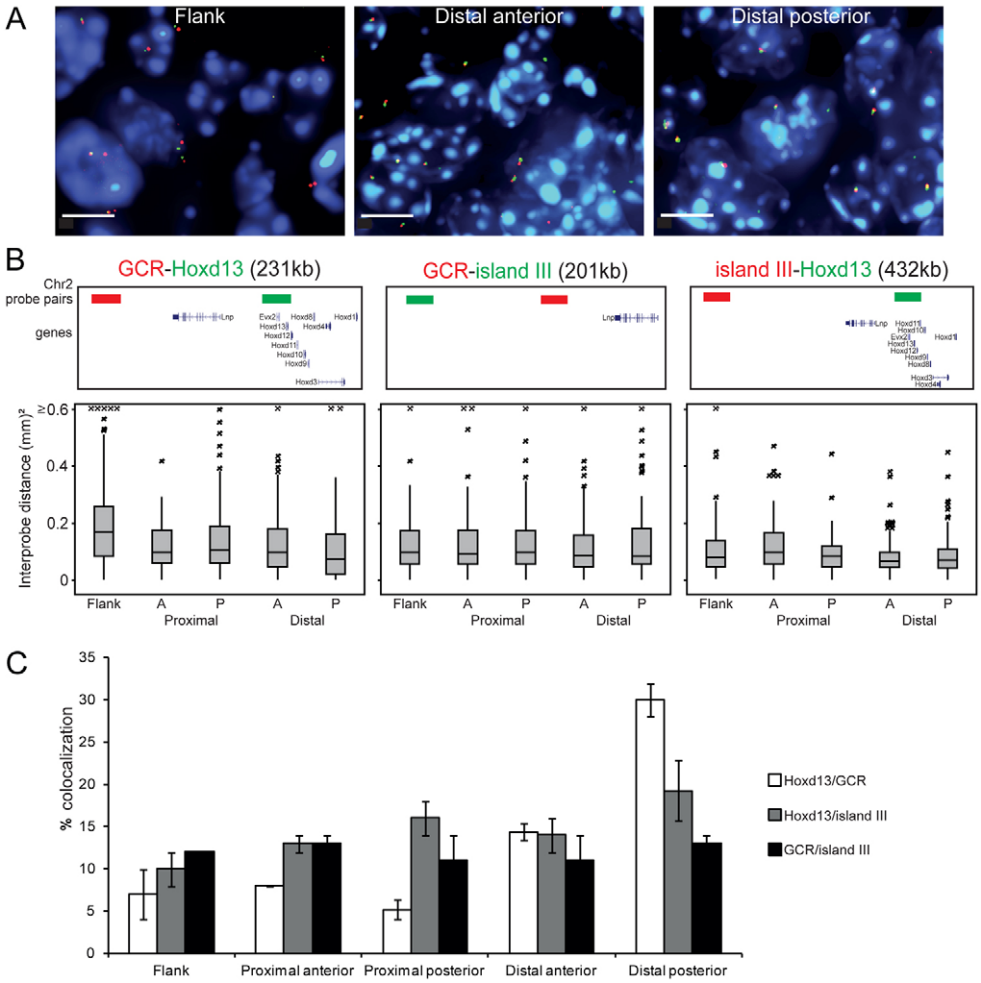

Fig. 7. GCR–5′ HoxD colocalisation at the E11 distal posterior mouse forelimb bud. (**A**) Nuclei from distal limb and flank tissue sections after FISH with GCR and 5′ HoxD probe pairs. Scale bars: 5 μm. (**B**) FISH with probe pairs: GCR–5′ HoxD, GCR–island III and 5′ HoxD–island III at distal and proximal forelimb bud and flank regions. $n \geq 100$ for each. Distribution of interprobe distances as in Fig. 6B and statistical analysis shown in supplementary material Table S7. (**C**) Percentage colocalised probe pairs (d<200 nm) for each of the genomic regions assayed in the distal anterior, distal posterior, proximal anterior, proximal posterior forelimb bud and the flank. n=100. Error bars indicate s.e.m. obtained from two different tissue sections. The statistical significance of the differences in colocalisation between the limb regions and the flank were examined by Fisher's exact test (supplementary material Table S8).

region is higher in distal limb than in the proximal region (Fig. 7; supplementary material Table S7). These data suggest that the entire ~400 kb genomic region from the 5′ end of HoxD into the centromeric gene desert is configured in a relatively compact, yet flexible, conformation.

DISCUSSION

Differential 5′ Hoxd gene expression across the limb A-P axis in mouse E10.5 embryos

We have shown that immortalised cell lines derived from the anterior versus posterior E10.5 distal limb sustain global expression patterns consistent with their mesenchymal origin from the limb during A-P axis specification (Fig. 1). Moreover, they maintain some of the differential Hoxd gene expression patterns of the temporal developmental stage from which they are derived (Fig. 2). Limb-specific secondary activation of HoxD initiates in the distal posterior forelimb bud at ~E10.5 in the mouse. We confirmed that 5′ *Hoxd* gene expression is significantly higher in distal posterior E10.5 cells relative to distal anterior (Fig. 2), commensurate with the spatial and temporal aspects of late phase collinearity (Spitz et al., 2003). This A-P difference is lost by E11.5-12.5 as the 5′ genes are activated in more distal anterior regions, but with *Hoxd13* still being the most strongly expressed (supplementary material Fig. S5) (Montavon et al., 2008).

A model for late phase HoxD activation in the distal limb proposes a reciprocal activation pathway involving restriction of earlier 5′ *Hoxd* expression to the posterior margin of the limb bud that then ensures posterior-only *Shh* activation, which in turn effects the initiation of secondary 5′ *Hoxd* expression in the distal posterior limb bud (Harfe et al., 2004; Robert and Lallemand, 2006). We did not detect *Shh* expression in either (P1 or P2) posterior-derived cell lines, which nonetheless maintain upregulated 5′ *Hoxd* gene expression, especially of *Hoxd13* (Fig. 2). However, late phase Hoxd gene expression still occurs in $Shh^{-/-}$ $Gli3^{-/-}$ mice, and is only reduced in $Shh^{-/-}$ mice (Litingtung et al., 2002). *Shh* expression prevents *Gli3* repression of 5′ Hoxd genes, both by repressing *Gli3* expression posteriorly and by antagonising Gli3 processing to Gli3R (repressor form). Gli3R has been suggested to be the repressor of 5′ Hoxd gene expression in anterior limb (Tarchini and Duboule, 2006). It is likely that posterior *Shh* expression in the embryonic limb, up to the point of cell immortalisation, was sufficient to activate late phase HoxD expression. The subsequent strong maintenance of *Hoxd13* expression in the posterior limb-derived cell lines suggests that *Shh* is not required for maintaining HoxD activity. Lack of *Shh* expression in cell lines could be due to the loss of interaction between the mesenchyme and the overlying AER (Laufer et al., 1994; Ogura et al., 1996).

Posteriorly restricted Hoxd expression is accompanied by chromatin decompaction and reduced polycomb binding

We identified differential H3K27me3 over 5′ Hoxd genes between anterior- and posterior-derived limb cell lines. In anterior cells, there is extensive H3K27me3 over *Hoxd13* towards *Hoxd10* that is

absent from posterior cells (Fig. 3). That this contributes to the repression of 5′ Hoxd genes in the anterior distal limb is consistent with the ectopic anterior expression of *Hoxd11* and *Hoxd13* in E10.5 limb buds after ablation of the PRC2 component Ezh2 (Wyngaarden et al., 2011). As Hoxd genes have been transcriptionally active during the earlier phase of limb development, we cannot determine whether there is active H3K27me3 removal from 5′ HoxD in cells of the posterior distal E10.5 limb, or re-establishment of H3K27me3 in anterior distal cells. The presence of H3K27me3 over 3′ HoxD in both anterior and posterior cell lines and in limb tissue probably represents a re-imposition of this histone mark after the initial phase of Hoxd gene expression in early, proximal limb bud development (Fig. 3).

Late phase 5′ Hoxd gene expression in the posterior distal limb bud is also accompanied by reduced Ring1B binding (Fig. 3; supplementary material Fig. S2). Consistent with a requirement for PRC1 to maintain Hox clusters in a silent, compact chromatin state in ES cells (Eskeland et al., 2010), we found differential chromatin compaction at HoxD both between the anterior- and posterior-derived limb cell lines and in limb tissue (Figs 5, 6), with a greater degree of decompaction in cells from the posterior distal region than in cells measured in any other region of the limb bud at this stage of development (Fig. 6). Our data suggest that dynamic polycomb-mediated control of HoxD expression and higher-order chromatin structure, previously described as occurring along the main A-P body axis (Morey et al., 2007; Soshnikova and Duboule, 2009) is recapitulated during limb-specific Hoxd gene expression.

Enhancer-promoter looping restricted to the posterior distal region of the limb bud

We observed a closer average proximity, and higher absolute colocalisation frequency, of the GCR to *Hoxd13* specifically at the distal posterior limb bud (Fig. 7; supplementary material Fig. S4A), consistent with the formation of a chromatin loop between enhancers of the GCR and the 5′ HoxD at the time and place of distal limb bud development when the GCR is involved in initiating HoxD quantitative collinearity and *Hoxd13* expression (Spitz et al., 2003; Montavon et al., 2008). Our analysis at single cell resolution is consistent with average interaction frequencies captured between the 5′ HoxD region and GCR by 4C analysis in the limb bud (Montavon et al., 2011), although there was no analysis of anterior versus posterior regions of the limb in that study. By contrast, we did not find significantly increased colocalisation of 5′ HoxD and a more distal regulatory region (island III) (Fig. 7C; supplementary material Fig. S4C) previously identified by 4C analysis. However, that study was conducted at a later developmental stage (E12.5) and any colocalisation might therefore occur later than E11. Our analysis does indicate that the ~400 kb region extending out from the 5′ HoxD locus into the adjacent gene desert is in a generally compact chromatin conformation in all the limb regions tested (Fig. 7A,B; supplementary material Table S7). Thus, the entire regulatory domain may be configured to minimise the nuclear search space for enhancer-gene interactions to then occur at the correct time and place. Further analyses over the entire temporal stage of late phase HoxD activity (E10.5-12.5) and across the A-P distal axis should clarify the spatial and temporal specificity of the multiple regulatory elements. We could not assess the colocalisation of the Prox regulatory element (Fig. 5A) as it is too close to *Hoxd13* for us to resolve by FISH.

This article demonstrates that complex higher-order chromatin dynamics is implicated in the regulation of Hoxd gene expression during distal limb development, with two different processes occurring: chromatin decompaction and looping. It also establishes immortomouse-derived cell lines as a tractable model system to investigate chromatin states in relation to spatiotemporally regulated gene expression in development. This is the first demonstration of differential chromatin compaction and enhancer-gene colocalisation across the A-P axis of the developing limb, as a previous study analysing the spatial colocalisation of *Shh* and its limb enhancer reported similar colocalisation in both posterior (*Shh*-expressing) and anterior (no *Shh* expression) limb regions (Amano et al., 2009).

Acknowledgements
We thank the Welcome Trust Clinical Research Facility (Western General Hospital, Edinburgh) for Illumina expression arrays.

Funding
This work was supported by the Medical Research Council, UK. Deposited in PMC for release after 6 months.

Competing interests statement
The authors declare no competing financial interests.

Supplementary material
Supplementary material available online at
http://dev.biologists.org/lookup/suppl/doi:10.1242/dev.081174/-/DC1

References

Amano, T., Sagai, T., Tanabe, H., Mizushina, Y., Nakazawa, H. and Shiroishi, T. (2009). Chromosomal dynamics at the Shh locus: limb bud-specific differential regulation of competence and active transcription. *Dev. Cell* **16**, 47-57.

Benjamini, Y. and Hochberg, Y. (1995). Controlling the false discovery rate: a practical and powerful approach to multiple testing. *J. Roy. Statist. Soc. B* **57**, 289-300.

Boyer, L. A., Plath, K., Zeitlinger, J., Brambrink, T., Medeiros, L. A., Lee, T. I., Levine, S. S., Wernig, M., Tajonar, A., Ray, M. K. et al. (2006). Polycomb complexes repress developmental regulators in murine embryonic stem cells. *Nat. Cell Biol.* **441**, 349-353.

Chambeyron, S. and Bickmore, W. A. (2004). Chromatin decondensation and nuclear reorganization of the HoxB locus upon induction of transcription. *Genes Dev.* **18**, 1119-1130.

Chambeyron, S., Da, Silva, N. R., Lawson, K. A. and Bickmore, W. A. (2005). Nuclear re-organisation of the Hoxb complex during mouse embryonic development. *Development* **132**, 2215-2223.

Condie, B. G. and Capecchi, M. R. (1993). Mice homozygous for a targeted disruption of Hoxd-3 (Hox-4.1) exhibit anterior transformations of the first and second cervical vertebrae, the atlas and the axis. *Development* **119**, 579-595.

Deschamps, J. and van Nes, J. (2005). Developmental regulation of the Hox genes during axial morphogenesis in the mouse. *Development* **132**, 2931-2942.

Duboc, V. and Logan, M. P. O. (2011). Regulation of limb bud initiation and limb-type morphology. *Dev. Dyn.* **240**, 1017-1027.

Dunning, M. J., Smith, M. L., Ritchie, M. E. and Tavaré, S. (2007). beadarray: R classes and methods for Illumina bead-based data. *Bioinformatics* **23**, 2183-2184.

Eden, E., Navon, R., Steinfeld, I., Lipson, D. and Yakhini, Z. (2009). GOrilla: a tool for discovery and visualization of enriched GO terms in ranked gene lists. *BMC Bioinformatics* **10**, 48.

Endoh, M., Endo, T. A., Endoh, T., Fujimura, Y.-I., Ohara, O., Toyoda, T., Otte, A. P., Okano, M., Brockdorff, N., Vidal, M. et al. (2008). Polycomb group proteins Ring1A/B are functionally linked to the core transcriptional regulatory circuitry to maintain ES cell identity. *Development* **135**, 1513-1524.

Eskeland, R., Leeb, M., Grimes, G. R., Kress, C., Boyle, S., Sproul, D., Gilbert, N., Fan, Y., Skoultchi, A. I., Wutz, A. et al. (2010). Ring1B compacts chromatin structure and represses gene expression independent of histone ubiquitination. *Mol. Cell* **38**, 452-464.

Faust, C., Lawson, K. A., Schork, N. J., Thiel, B. and Magnuson, T. (1998). The Polycomb-group gene eed is required for normal morphogenetic movements during gastrulation in the mouse embryo. *Development* **125**, 4495-4506.

Harfe, B. D., Scherz, P. J., Nissim, S., Tian, H., McMahon, A. P. and Tabin, C. J. (2004). Evidence for an expansion-based temporal Shh gradient in specifying vertebrate digit identities. *Cell* **118**, 517-528.

Hill, R. E. (2007). How to make a zone of polarizing activity: insights into limb development via the abnormality preaxial polydactyly. *Dev. Growth Differ.* **49**, 439-448.

Jat, P. S., Noble, M. D., Ataliotis, P., Tanaka, Y., Yannoutsos, N., Larsen, L. and Kioussis, D. (1991). Direct derivation of conditionally immortal cell lines

from an H-2Kb-tsA58 transgenic mouse. *Proc. Natl. Acad. Sci. USA* **88**, 5096-5100.

Kohn, E. A., Du, Z., Sato, M., Van Schyndle, C. M., Welsh, M. A., Yang, Y.-A., Stuelten, C. H., Tang, B., Ju, W., Bottinger, E. P. et al. (2010). A novel approach for the generation of genetically modified mammary epithelial cell cultures yields new insights into TGFβ signaling in the mammary gland. *Breast Cancer Res.* **12**, R83.

Krawchuk, D. and Kania, A. (2008). Identification of genes controlled by LMX1B in the developing mouse limb bud. *Dev. Dyn.* **237**, 1183-1192.

Kuijper, S., Beverdam, A., Kroon, C., Brouwer, A., Candille, S., Barsh, G. and Meijlink, F. (2005). Genetics of shoulder girdle formation: roles of Tbx15 and aristaless-like genes. *Development* **132**, 1601-1610.

Laufer, E., Nelson, C. E., Johnson, R. L., Morgan, B. A. and Tabin, C. (1994). Sonic hedgehog and Fgf-4 act through a signaling cascade and feedback loop to integrate growth and patterning of the developing limb bud. *Cell* **79**, 993-1003.

Lee, T. I., Jenner, R. G., Boyer, L. A., Guenther, M. G., Levine, S. S., Kumar, R. M., Chevalier, B., Johnstone, S. E., Cole, M. F., Isono, K.-I. et al. (2006). Control of developmental regulators by Polycomb in human embryonic stem cells. *Cell* **125**, 301-313.

Lettice, L. A, Williamson, I., Wiltshire, J. H., Peluso, S., Devenney, P. S., Hill, A. E., Essafi, A., Hagman, J., Mort, R., Grimes, G. et al. (2012). Opposing functions of the ETS factor family define Shh spatial expression in limb buds and underlie polydactyly. *Dev. Cell* **22**, 459-467.

Litingtung, Y., Dahn, R. D., Li, Y., Fallon, J. F. and Chiang, C. (2002). Shh and Gli3 are dispensable for limb skeleton formation but regulate digit number and identity. *Nature* **418**, 979-983.

Lizarraga, G., Ferrari, D., Kalinowski, M., Ohuchi, H., Noji, S., Kosher, R. A. and Dealy, C. N. (1999). FGFR2 signaling in normal and limbless chick limb buds. *Dev. Genet.* **25**, 331-338.

Mao, J., McGlinn, E., Huang, P., Tabin, C. J. and McMahon, A. P. (2009). Fgf-dependent Etv4/5 activity is required for posterior restriction of Sonic Hedgehog and promoting outgrowth of the vertebrate limb. *Dev. Cell* **16**, 600-606.

Mizusawa, N., Hasegawa, T., Ohigashi, I., Tanaka-Kosugi, C., Harada, N., Itakura, M. and Yoshimoto, K. (2004). Differentiation phenotypes of pancreatic islet beta- and alpha-cells are closely related with homeotic genes and a group of differentially expressed genes. *Gene* **331**, 53-63.

Montavon, T., Le Garrec, J.-F., Kerszberg, M. and Duboule, D. (2008). Modeling Hox gene regulation in digits: reverse collinearity and the molecular origin of thumbness. *Genes Dev.* **22**, 346-359.

Montavon, T., Soshnikova, N., Mascrez, B., Joye, E., Thevenet, L., Splinter, E., de Laat, W., Spitz, F. and Duboule, D. (2011). A regulatory archipelago controls hox genes transcription in digits. *Cell* **147**, 1132-1145.

Morey, C., Da Silva, N. R., Perry, P. and Bickmore, W. A. (2007). Nuclear reorganisation and chromatin decondensation are conserved, but distinct, mechanisms linked to Hox gene activation. *Development* **134**, 909-919.

Morey, C., Kress, C. and Bickmore, W. A. (2009). Lack of bystander activation shows that localization exterior to chromosome territories is not sufficient to up-regulate gene expression. *Genome Res.* **19**, 1184-1194.

Ogura, T., Alvarez, I. S., Vogel, A., Rodríguez, C., Evans, R. M. and Izpisúa-Belmonte, J. C. (1996). Evidence that Shh cooperates with a retinoic acid inducible co-factor to establish ZPA-like activity. *Development* **122**, 537-542.

Pradeepa, M. M., Sutherland, H. G., Ule, J., Grimes, G. R. and Bickmore, W. A. (2012). Psip1/Ledgf p52 binds methylated histone H3K36 and splicing factors and contributes to the regulation of alternative splicing. *PLoS Genet*. **8**, e1002717.

Robert, B. and Lallemand, Y. (2006). Anteroposterior patterning in the limb and digit specification: contribution of mouse genetics. *Dev. Dyn.* **235**, 2337-2352.

Smyth, G. K., Michaud, J. and Scott, H. S. (2005). Use of within-array replicate spots for assessing differential expression in microarray experiments. *Bioinformatics* **21**, 2067-2075.

Soshnikova, N. and Duboule, D. (2009). Epigenetic temporal control of mouse Hox genes in vivo. *Science* **324**, 1320-1323.

Spitz, F., Gonzalez, F. and Duboule, D. (2003). A global control region defines a chromosomal regulatory landscape containing the HoxD cluster. *Cell* **113**, 405-417.

Spitz, F., Herkenne, C., Morris, M. A. and Duboule, D. (2005). Inversion-induced disruption of the Hoxd cluster leads to the partition of regulatory landscapes. *Nat. Genet.* **37**, 889-893.

Stock, J. K., Giadrossi, S., Casanova, M., Brookes, E., Vidal, M., Koseki, H., Brockdorff, N., Fisher, A. G. and Pombo, A. (2007). Ring1-mediated ubiquitination of H2A restrains poised RNA polymerase II at bivalent genes in mouse ES cells. *Nat. Cell Biol.* **9**, 1428-1435.

Tarchini, B. and Duboule, D. (2006). Control of Hoxd genes' collinearity during early limb development. *Dev. Cell* **10**, 93-103.

Tschopp, P. and Duboule, D. (2011). A regulatory "landscape effect" over the HoxD cluster. *Dev. Biol.* **351**, 288-296.

Vickerman, L., Neufeld, S. and Cobb, J. (2011). Shox2 function couples neural, muscular and skeletal development in the proximal forelimb. *Dev. Biol.* **350**, 323-336.

Voncken, J. W., Roelen, B. A. J., Roefs, M., de Vries, S., Verhoeven, E., Marino, S., Deschamps, J. and van Lohuizen, M. (2003). Rnf2 (Ring1b) deficiency causes gastrulation arrest and cell cycle inhibition. *Proc. Natl. Acad. Sci. USA* **100**, 2468-2473.

Williamson, I., Hill, R. E. and Bickmore, W. A. (2011). Enhancers: from developmental genetics to the genetics of common human disease. *Dev. Cell* **21**, 17-19.

Wyngaarden, L. A., Delgado-Olguin, P., Su, I.-H., Bruneau, B. G. and Hopyan, S. (2011). Ezh2 regulates anteroposterior axis specification and proximodistal axis elongation in the developing limb. *Development* **138**, 3759-3767.

Zakany, J. and Duboule, D. (2007). The role of Hox genes during vertebrate limb development. *Curr. Opin. Genet. Dev.* **17**, 359-366.

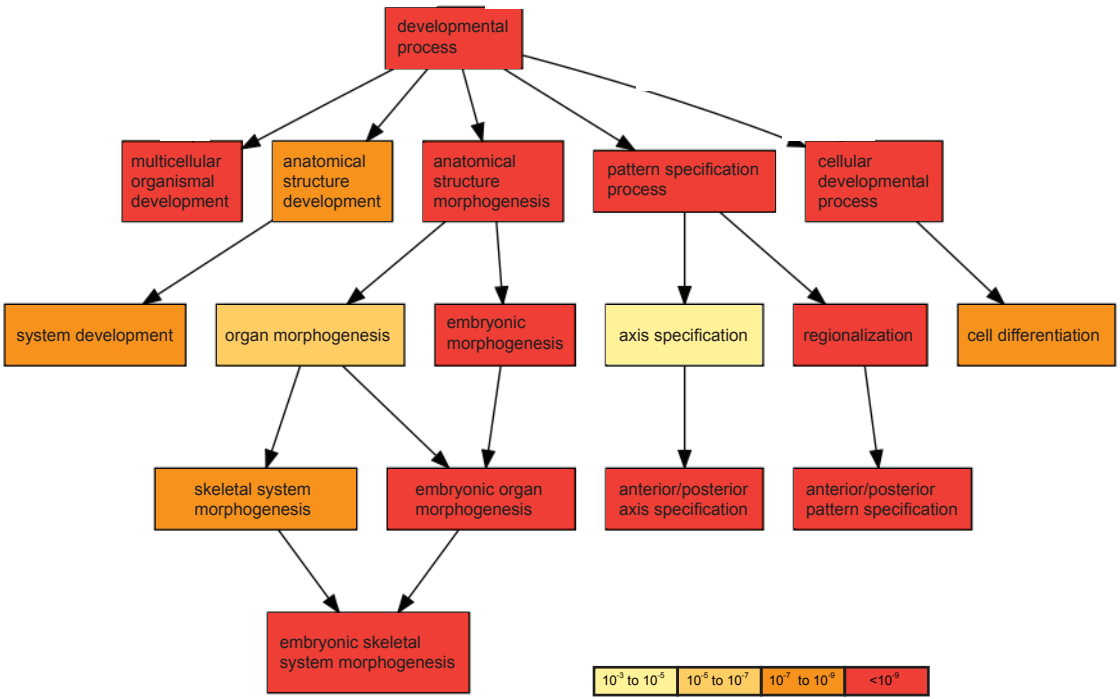
developmental process
multicellular organismal development
anatomical structure development
anatomical structure morphogenesis
pattern specification process
cellular developmental process
system development
organ morphogenesis
embryonic morphogenesis
axis specification
regionalization
cell differentiation
skeletal system morphogenesis
embryonic organ morphogenesis
anterior/posterior axis specification
anterior/posterior pattern specification
embryonic skeletal system morphogenesis
10^-3 to 10^-5
10^-5 to 10^-7
10^-7 to 10^-9
<10^-9

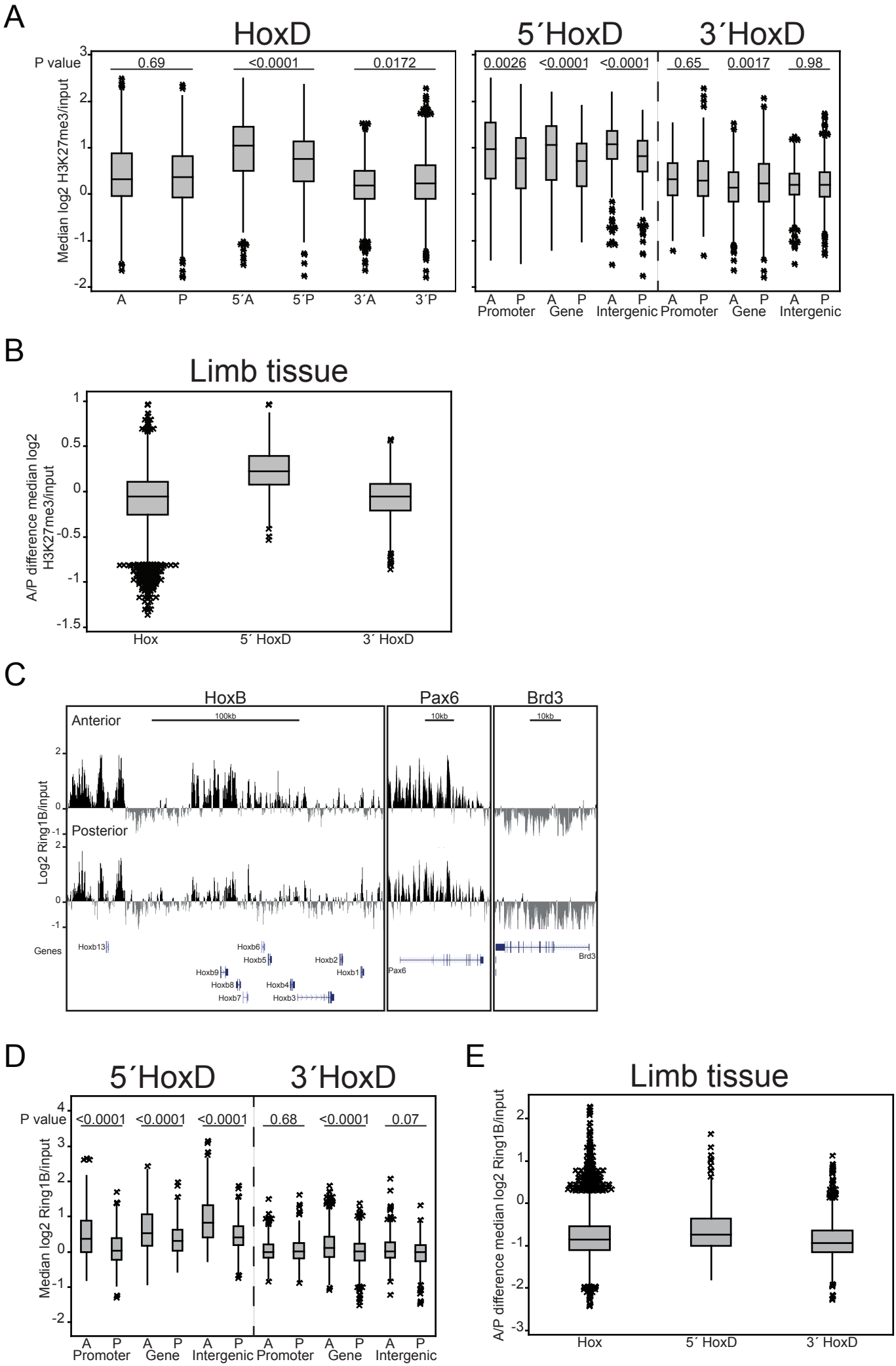
A
HoxD
5´HoxD
3´HoxD
P value
0.69
<0.0001
0.0172
0.0026
<0.0001
<0.0001
0.65
0.0017
0.98
Median log2 H3K27me3/input
A
P
5´A
5´P
3´A
3´P
Promoter
Gene
Intergenic
B
Limb tissue
A/P difference median log2 H3K27me3/input
Hox
5´ HoxD
3´ HoxD
C
HoxB
Pax6
Brd3
Anterior
Posterior
100kb
10kb
Log2 Ring1B/input
Genes
Hoxb13
Hoxb6
Hoxb5
Hoxb2
Hoxb9
Hoxb1
Hoxb8
Hoxb4
Hoxb7
Hoxb3
Pax6
Brd3
D
5´HoxD
3´HoxD
P value
<0.0001
<0.0001
<0.0001
0.68
<0.0001
0.07
Median log2 Ring1B/input
Promoter
Gene
Intergenic
E
Limb tissue
A/P difference median log2 Ring1B/input
Hox
5´ HoxD
3´ HoxD

A

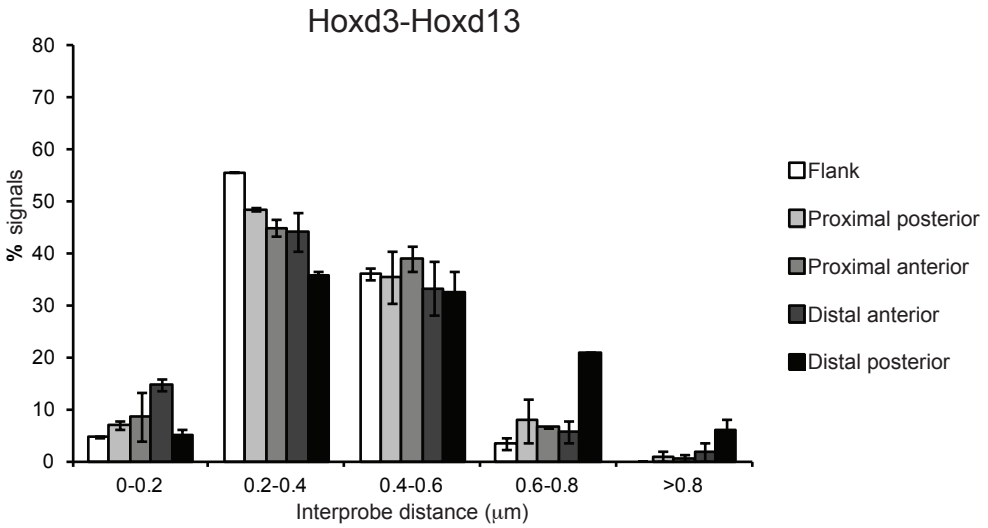
Hoxd3-Hoxd13
% signals
80
70
60
50
40
30
20
10
0
0-0.2
0.2-0.4
0.4-0.6
0.6-0.8
>0.8
Interprobe distance (μm)
Flank
Proximal posterior
Proximal anterior
Distal anterior
Distal posterior

B

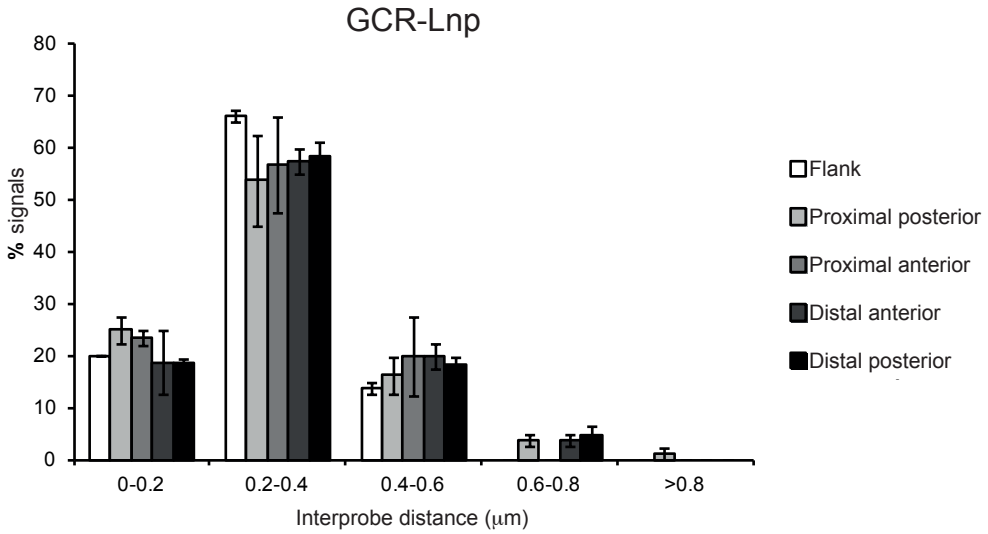
GCR-Lnp
% signals
80
70
60
50
40
30
20
10
0
0-0.2
0.2-0.4
0.4-0.6
0.6-0.8
>0.8
Interprobe distance (μm)
Flank
Proximal posterior
Proximal anterior
Distal anterior
Distal posterior

C

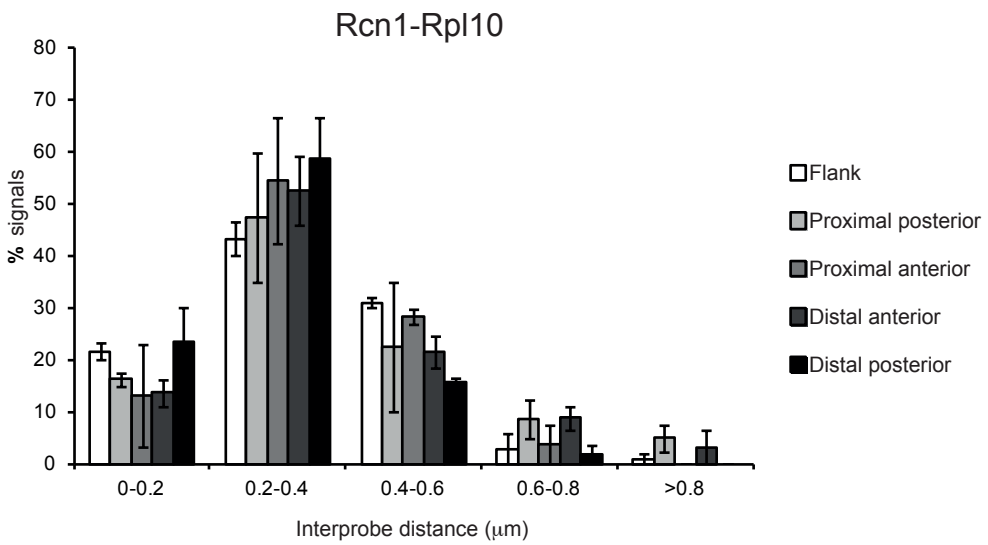
Rcn1-Rpl10
% signals
80
70
60
50
40
30
20
10
0
0-0.2
0.2-0.4
0.4-0.6
0.6-0.8
>0.8
Interprobe distance (μm)
Flank
Proximal posterior
Proximal anterior
Distal anterior
Distal posterior

A

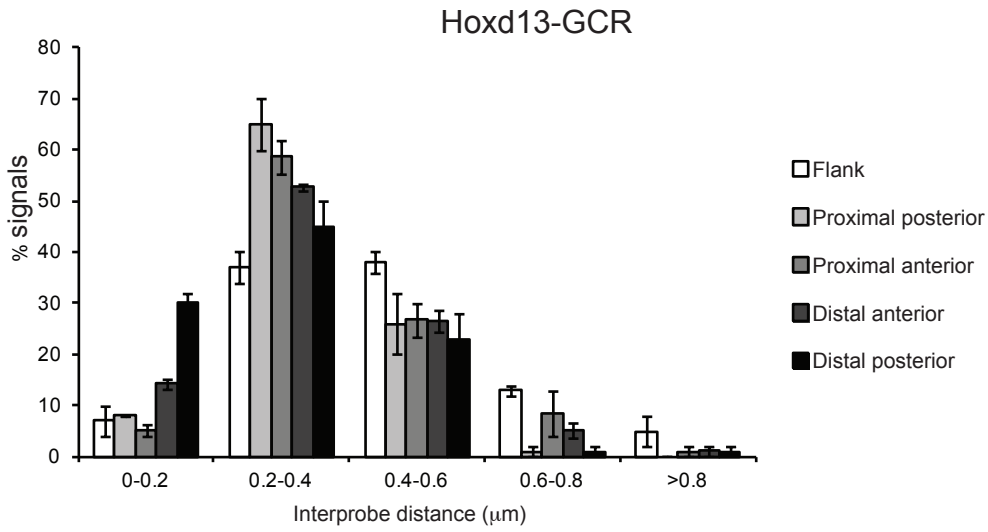
Hoxd13-GCR
% signals
80
70
60
50
40
30
20
10
0
0-0.2
0.2-0.4
0.4-0.6
0.6-0.8
>0.8
Interprobe distance (μm)
Flank
Proximal posterior
Proximal anterior
Distal anterior
Distal posterior

B

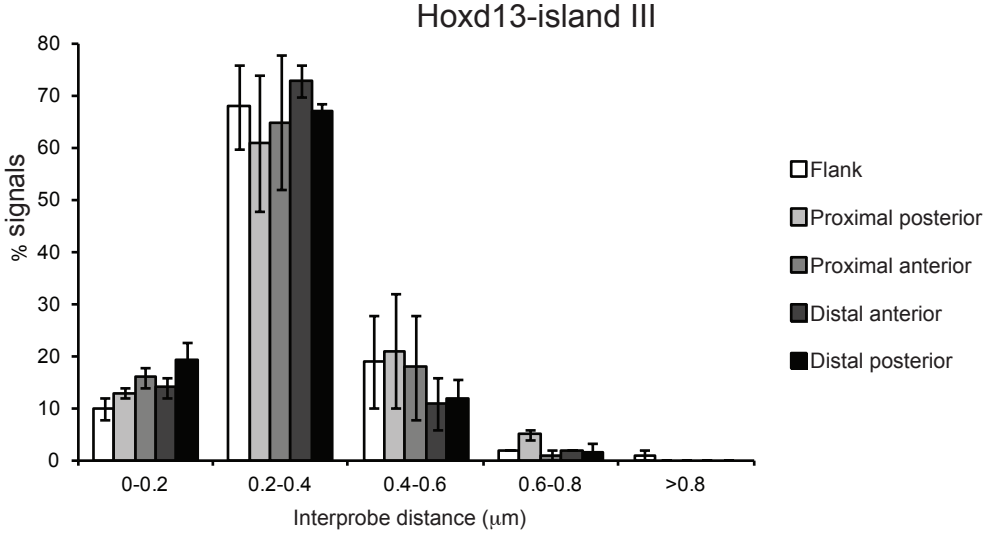
Hoxd13-island III
% signals
80
70
60
50
40
30
20
10
0
0-0.2
0.2-0.4
0.4-0.6
0.6-0.8
>0.8
Interprobe distance (μm)
Flank
Proximal posterior
Proximal anterior
Distal anterior
Distal posterior

C

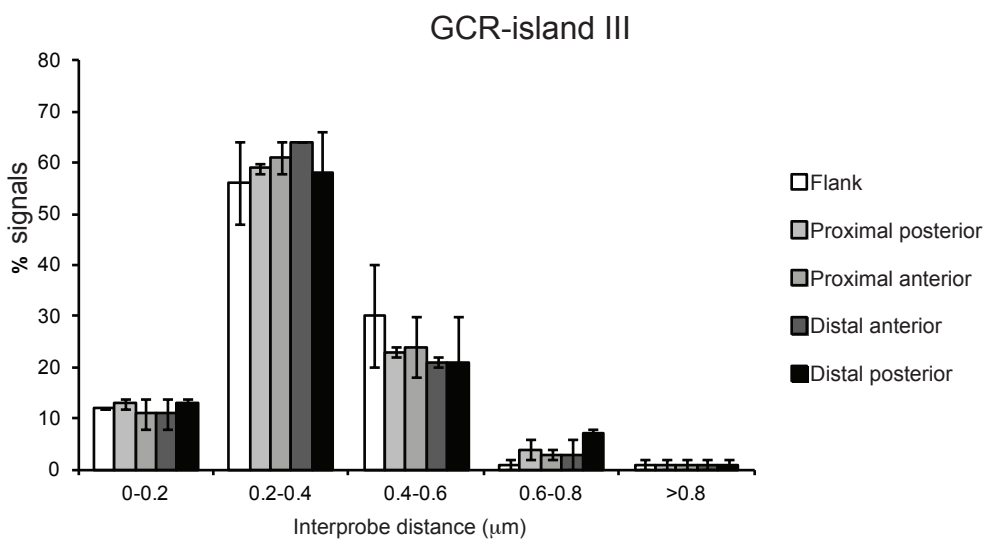
GCR-island III
% signals
80
70
60
50
40
30
20
10
0
0-0.2
0.2-0.4
0.4-0.6
0.6-0.8
>0.8
Interprobe distance (μm)
Flank
Proximal posterior
Proximal anterior
Distal anterior
Distal posterior

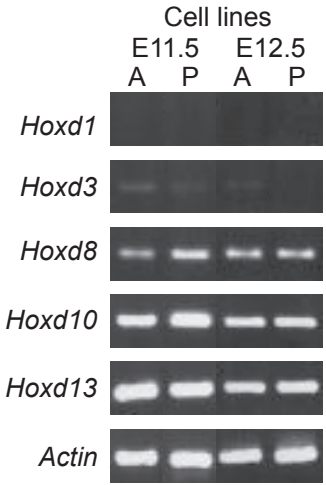
Cell lines
E11.5
E12.5
A
P
A
P
Hoxd1
Hoxd3
Hoxd8
Hoxd10
Hoxd13
Actin

Table S1. Real-time PCR primers for analysis of transcript levels

Gene	Oligo name	Sequence	Reference
Hoxd1	d1bUp	CCACAGCACTTTCGAGTGGA	Morey et al., 2007
Hoxd1	Hoxd1r	ACTCTTTCTCTAGCTCTGTCAG	
Hoxd3	d3pA	GAACTCCAAGCAGAAGAACAG	Condie and Capecchi, 1993
Hoxd3	Hoxd3r	CAGATAGCGGTTGAAGTGGAAC	
Hoxd4	Hoxd4f	GGAGAACGAGGGAGAACCA	
Hoxd4	Hoxd4r	TCTGCTGCTGCTATGACTGC	
Hoxd8	Hoxd8f	CACTTAAATCAGAGCTCGTCTCC	
Hoxd8	Hoxd8r	GACCTCGATTCTCCTCTTCCTGG	
Hoxd10	Hoxd10f	GTGCAGGAGAAGGAAAGCAAAG	Modified from Mizusawa et al., 2004
Hoxd10	Hoxd10r	TAACGCTCTTACTGATCTCTAGGC	
Hoxd11	Hoxd11f	TCCAGGCAAACGAGAGAAAC	
Hoxd11	Hoxd11r	TTGGCAAATAAGGTTTCTGGA	
Hoxd12	Hoxd12f	CAACTTGAACATGGCAGTGCAAG	
Hoxd12	Hoxd12r	CTGCTGCTTTGTGTAGGGTTTCC	
Hoxd13	Hoxd13f	AGTCCTGGACGCTAGCCAACG	
Hoxd13	Hoxd13r	GTAGACGCACATGTCCGGCTG	
Actin	Actinf	AGAGCTATGAGCTGCCTGACG	
Actin	Actinr	TGTGTTGGCATAGAGGTCTTTACG	
Lnp	LnpaUp	GTGGAAGGCTCAAGCTCAAC	
Lnp	LnpbLo	TGCTGGGCAATCTGAATATG	
GAPDH	GABDHf	ATCACCATCTTCCAGGAGCGAG	
GAPDH	GABDHr	GACCCTTTTGGCTCCACCCTTC	Modified from Boyer et al., 2006
FgfR2b	FGFR2f	CTGTTCAATGTGACGGAGATGG	
FgfR2b	FGFR2r	ACAGACGCGTTGTTAYCCTCAC	
FgfR2c	FGF2Cf	CACTCTGCATGGTTGACAGTTC	
FgfR2c	FGF2Cr	CACTCTGCATGGTTGACAGTTC	
Fgf8	FGF8f	AAAGTCACACAGCGACATGTGAGG	
Fgf8	FGF8r	TCTGTGAATACGCAGTCCTTGCCT	
Fgf10	FGF10f	AGCGGGACCAAGAATGAAGACTGT	
Fgf10	FGF10r	CCTGCCATTGTGCTGCCAGTTAAA	
Etv4	Pea3f	ACCATGGAGAGCAGTGCCTTTACT	
Etv4	Pea3r	ATGCACATCCAGGGACATCTGAGT	

Table S2. Real-time PCR primers for ChIP analysis of promoter regions

Promoter/exon	Oligo name	Sequence	Reference
Hoxd1	Hoxd1promf	GAGTAACTTGACCTTCTCAGAG	
	Hoxd1promr	ATTGCGGGAGAAAGGCAGGGAAG	
Hoxd10	Hoxd10prof	TAGTAGATGTCGCTGTTGTCCG	
	Hoxd10pror	ACATGACAACCAAGCCAATGAGA	
Olig2	Olig2f	GCCTGACGCTACAGTGACAA	Boyer et al., 2006
	Olig2r	GGCTAATTCCGCTCAATGAA	Boyer et al., 2006
Actin	Actinf	CCTCGATGCTGACCCTCATCC	
	Actinr	GACACTGCCCCATTCAATGTCTC	

Table S3. Fosmid probes

	Region	Whitehead (Sanger) name	Ensemble name	Coordinates		Size (bp)
				Start	End	
Hoxd	*GCR**	WI1-2157A11	G135P63331H7	74242615	74282044	39,429
	*Lnp**	WI1-482L15	G135P61870C5	74329582	74372986	43,404
	*Evx2-Hoxd13**	WI1-469P2	G135P67444A12	74474157	74513003	38,846
	*Hoxd4-Hoxd1**	WI1-121N10	G135P67844B8	74566983	74605438	38,455
	Island III	WI1-1404J11	G135P64810D7	74040543	74081331	40,788
Pax6	*Rcn***	WI1-1767E4	G135P601417F11	105221381	105259938	38,557
	*Rpl10***	WI1-1550J22	G135P601672D2	105387894	105425103	37,209

Names are Ensembl (r 45) (http://jun2007.archive.ensembl.org/Mus_musculus/index.html). Mouse genome assembly number: NCBI m37.
Asterisks indicate fosmids previously used in *Morey et al., 2007; Morey et al., 2009; **and Eskeland et al., 2010.

Table S4. Normalised interprobe distance for A1 & P1 and A2 & P2 cell lines

Cell line	*Hoxd3-Hoxd13* (93 kb)	GCR-*Lnp* (89 kb)	*Rcn-Rpl10* (166 kb)
	Normalized interprobe distance (d^2/r^2)		
A1	0.0056	0.0021	0.0039
P1	0.0084 (*P*=0.0002)	0.0024 (*P*=0.05)	0.0030 (*P*=0.11)
A2	0.0060	0.0025	0.0054
P2	0.0084 (*P*=0.03)	0.0027 (*P*=0.90)	0.0038 (*P*=0.08)
	Squared interprobe distance (d^2) (μm^2)		
A1	0.16	0.066	0.11
P1	0.25 (*P*<0.0001)	0.073 (*P*=0.34)	0.09 (*P*=0.14)
A2	0.20	0.09	0.18
P2	0.27 (*P*=0.02)	0.08 (*P*=0.88)	0.12 (*P*=0.10)

Statistical analysis of data for Fig. 4. Interprobe distances are median values; *P*-values from Mann-Whitney U tests.

Table S5. Interprobe distances for E11 limb bud sections

Limb region	*Hoxd3-Hoxd13* (93 kb)	GCR-*Lnp* (89 kb)	*Rcn-Rpl10* (166 kb)
	Interprobe distance (d^2) (μm^2)		
Distal posterior	0.178	0.076	0.080
Distal anterior	0.116 (*P*=0.0008)	0.076 (*P*=0.93)	0.081 (*P*=0.10)
Proximal posterior	0.153 (*P*=0.02)	0.076 (*P*=0.46)	0.090 (*P*=0.06)
Proximal anterior	0.098 (*P*=0.0002)	0.074 (*P*=0.45)	0.112 (*P*=0.05)
Flank	0.130 (*P*=0.0002)	0.078 (*P*=0.49)	0.112 (*P*=0.17)

Statistical analysis of data for Fig. 5. Interprobe distances are median values, *P*-values from Mann-Whitney U tests.

Table S6. Frequency of HoxD GCR and *Pax6* apposite probes separated by ≥ 600 nm for E11 limb bud sections

Limb region	*Hoxd3-Hoxd13* (93 kb)	GCR-*Lnp* (89 kb)	*Rcn-Rpl10* (166 kb)
	Frequency (%) ≥ 600 nm		
Distal posterior	27	5	4
Distal anterior	8 (*P*=0.0001)	4 (*P*=1.00)	12 (*P*=0.02)
Proximal posterior	7 (*P*=0.0001)	0 (*P*=0.12)	4 (*P*=0.44)
Proximal anterior	9 (*P*=0.001)	5 (*P*=1.00)	14 (*P*=0.009)
Flank	3.5 (*P*=0.0001)	0 (*P*=0.12)	4 (*P*=0.44)

Statistical analysis of data for Fig. S3. *P*-values from Fisher's exact tests.

Table S7. Interprobe distances for HoxD regulatory regions in E11 limb bud sections

Limb region	*Hoxd13*-GCR (231 kb)	Island III-GCR (201 kb)	*Hoxd13*-island III (432 kb)
	Interprobe distance (d^2) (μm^2)		
Distal posterior	0.076	0.084	0.072
Distal anterior	0.098 (*P*=0.04)	0.087 (*P*=0.43)	0.067 (*P*=0.96)
Proximal posterior	0.107 (*P*=0.002)	0.098 (*P*=0.99)	0.085 (*P*=0.11)
Proximal anterior	0.098 (*P*=0.02)	0.094 (*P*=1.00)	0.099 (*P*=0.005)
Flank	0.171 (*P*=0.0001)	0.098 (*P*=0.77)	0.081 (*P*=0.04)

Statistical analysis of data for Fig. 6B. Interprobe distances are median values; *P*-values from Mann-Whitney U tests.

Table S8. Colocalisation frequency of 5′ HoxD and enhancer probes for E11 limb bud sections

Limb region	*Hoxd13*-GCR (231 kb)	Island III-GCR (201 kb)	*Hoxd13*-island III (432 kb)
	Colocalisation frequency (%)		
Distal posterior	30	13	19
Distal anterior	14 (*P*=0.01)	11 (*P*=0.83)	14 (*P*=0.30)
Proximal posterior	5 (*P*<0.0001)	11 (*P*=0.839)	16 (*P*=0.61)
Proximal anterior	8 (*P*=0.0001)	13 (*P*=1.00)	13 (*P*=0.22)
Flank	7 (*P*<0.0001)	12 (*P*=1.00)	10 (*v*0.07)

Statistical analysis of data for Fig. 6C. *P*-values from Fisher's Exact tests.